J Solid State Electrochem (2001) 5: 402–411
DOI 10.1007/s100080000169

ORIGINAL PAPER

Peter Mayer · Rudolf Holze

Electrocatalysis of redox reactions by metal nanoparticles on graphite electrodes

Received: 23 June 2000 / Accepted: 21 August 2000 / Published online: 16 May 2001

Abstract A selection of graphitic materials of both scientific as well as commercial importance has been modified by deposition of various metals at very low coverages under overpotential or underpotential conditions. Nanoparticles were found with some metals. The changes in the electrocatalytic activity of the supporting electrode by the metal modification were studied using electrochemical impedance measurements of a fast redox system. The carbon/solution interface was characterized with surface Raman spectroscopy, electrochemical impedance measurements, and cyclic voltammetry.

Keywords Electrocatalysis · Modified electrodes · Redox batteries

Introduction

Catalytic properties of graphitic electrodes are not adequate for many electrochemical processes of technological interest like, e.g., electrolytical processes [1, 2]. Their activity can be enhanced considerably by modification of the graphite surface with metal deposits [3, 4, 5, 6, 7, 8, 9, 10, 11, 12, 13, 14, 15]. These metals have been added sometimes just in minute amounts as soluble salts to electrolyte solutions as, e.g., employed in fuel cells. Besides these applications, the use of modified graphitic materials in redox batteries has been tested [18, 19, 20, 21]. The fundamentals of redox batteries have been presented previously [22, 23, 24, 25, 26, 27, 28].

The modifying metals may be present as overpotential deposits (opd, i.e., deposited at electrode potentials negative to the Nernst potential of the deposited metal assuming that the metal ion and the metal itself form the redox electrode) or underpotential deposits (i.e., deposited at electrode potentials positive to this Nernst potential). Sometimes the deposition of the metal results just in an increase of the electrochemically active surface area; the increase in the electrode current at a given electrode potential is consequently not caused by enhanced electrocatalysis. Separation of this surface enlargement effect from truly catalytic effects is of fundamental importance.

This report presents the results of kinetic investigations with various graphitic materials of both commercial as well as scientific interest:

1 Glassy carbon (electrochemically activated),
2 Elektrodengraphit EH (a porous material containing vanadium),
3 Pyrolytic graphite[1],
4 Diabon N (a graphitized, polymer-bonded material), and
5 Ridurid (a non-porous material bonded with phenolic resin).

In order to obtain a picture of the surface topography, selected systems were subjected to scanning electron microscopy. Surface Raman spectroscopy was employed to obtain information about the degree of ordering of the surface.

A review of the published reports on kinetic data of redox reactions at various carbon-based electrode surfaces yields pertinent data for various redox reactions as measured with highly ordered pyrolytic graphite and glassy carbon [29]. As a major factor influencing electron transfer physico-chemical properties like, e.g., density of electronic states (lower with the former material) were identified. The iron redox couple investigated here has been studied before together with other redox systems by McDermott et al. [30].

Rate constants k^0 have been found to be always greater for less ordered materials. Electrochemical

Paper presented at the 50th ISE Meeting, Pavia, Italy, September 5–10, 1999

P. Mayer · R. Holze (✉)
Technische Universität Chemnitz,
Institut für Chemie, 09107 Chemnitz, Germany
E-mail: rudolf.holze@chemie.tu-chemnitz.de

[1]Sometimes this material is also called ordinary pyrolytic graphite OPG

activation by exposing the electrode to electrode potential cycling in a suitable electrolyte solution as also employed here has resulted in considerable increases of the rate of reaction. Kinetic data for the $Fe^{2+/3+}$ system in an aqueous electrolyte solution of 1 M HCl have been reported by Hollax and Cheng [31].

Materials and methods

Five different types of graphitic materials were used: Pyrolytic graphite (Ringsdorff; PG), glassy carbon (Ringsdorff; GC), Elektrodengraphit EH (Sigri; EG), Diabon N (Sigri; Dia), and Ridurid V 1017 (Ringsdorff, RID). The first and second material are composed of carbon only and prepared by various means (deposition from gaseous hydrocarbons on a hot surface and pyrolysis of synthetic polymers). The other materials are composites made of graphite and various binding materials, they show slightly different values of density. Elektrodengraphit EH contains some vanadium, it is also somewhat porous. The samples were cut into discs of 0.282 cm^2 apparent surface area. The discs were glued onto copper rods with conductive silver or graphite (in case of the porous Elektrodengraphit EH) cement and embedded in epoxy (Ciba-Geigy Araldit D/HY 956). For comparison, electrodes of highly ordered pyrolytic graphite (HOPG-ZYH, Advanced Ceramics, USA) with the basal and the edge plane exposed were used.

Before electrochemical measurements the electrodes were polished with γ-Al_2O_3 of 0.3 mm and 0.05 mm grain size (Bühler Micropolish). Subsequently, they were rinsed twice with ultrapure water (Seralpur pro 90c) and sonicated twice for ten minutes in order to remove traces of the polishing powder.

Glassy carbon electrodes were activated electrochemically in an H-cell filled with 1 M sulfuric acid by applying ten electrode potential cycles between $-0.36\ V < E_{RHE} < 2.1\ V$ at a scan rate of $dE/dt = 50\ mV\ s^{-1}$. After activation the electrode was rinsed again with ultrapure water. Changes effected by this procedure and its effects have been discussed elsewhere [32, 33, 34, 35, 36].

Metal deposit modification was done by applying two potential cycles starting and ending at the negative potential limit. 1 M solutions of $HClO_4$ with 10^{-3} **M** $Ni(NO_3)_2$, $Tl(NO_3)_2$, $Pd(NO_3)_2$, $Bi(NO_3)_3$, $In(NO_3)_3$, $NaPt(CN)_6$, (all salts supplied by Strem Chemicals), $Sn(CH_3COO)_2$, $Cu(CH_3COO)_2$, $AgCH_3COO$), $Cd(CH_3COO)_2$, $Co(CH_3COO)_2$ (p.A., Riedel de Haen) were used. The slow cathodic going potential scan ($dE/dt = 5\ mV\ s^{-1}$) was stopped at an electrode potential negative to the opd/upd peak.

The charge consumed during metal deposition was obtained by integrating the cathodic peak in experiments with smooth, polished electrodes. A gold wire counter electrode and a hydrogen reference electrode filled with the supporting electroyte solution were used. All electrode potentials are quoted versus this reference.

Electrolyte solutions were prepared from 18 MW water (Seralpur pro 90c) with 0.1 and 1 M $HClO_4$. All electrochemical experiments were performed at room temperature using solutions purged with nitrogen.

Impedance measurements were done with a transfer function analyser Solartron SI 1255 and a potentiostat (Solartron SI 1287) at the spontaneously established rest potential E_0 of the used redox system [1 **M** $HClO_4 + 10^{-2}$ **M** $(NH_4)_2Fe(SO_4)_2$ (Riedel de Haen) + 10^{-2} **M** $(NH_4)Fe(SO_4)_2$ (Merck)]. The electrochemical cell was designed keeping its AC-behaviour in mind as has been described elsewhere [37, 38]. A hydrogen reference electrode filled with 1 M $HClO_4$ solution and a platinum sheet counter electrode were used. Evaluation of the data was done with the help of the software provided by Boukamp (V. 3.97).

Cyclic voltammetry was used to establish the exchange current density in separate experiments independently of the impedance measurements. Scans were run using custom developed software and the potentiostat (Solartron SI 1287) as above. Evaluation of the cyclic voltammograms followed standard procedures [39].

Surface Raman spectra of the investigated materials (including activated glassy carbon) were recorded on an ISA 64000 spectrometer equipped with a liquid nitrogen cooled CCD camera detector at a resolution of 2 cm^{-1}. Samples were illuminated with laser light provided by Coherent Innova 70 systems. Further experimental details are provided in the figure captions. Observed shifts of the band around $\bar{\nu} = 1355\ cm^{-1}$ attributed to the D or A_{1g} mode of graphite (see below) as a function of the excitation wavelength [40] were not taken into account. Electrodes made of composite materials were illuminated with laser light of $\lambda_0 = 647$ nm in order to reduce unwanted fluorescence.

Scanning electron microscope pictures were obtained with a Philips SEM 1515 microscope.

Results and discussion

A typical cyclic voltammogram (CV) as observed with an electrode made of Elektrodengraphit EH during modification of the electrode by deposition of lead is displayed in Fig. 1. The two cathodic current waves can be assigned to the upd-process at about $E_{RHE} = 0.62$ V and to the bulk deposition around $E_{RHE} = -0.21$ V. The reversibility of the upd-process can be visualised more easily by recording a CV with slightly closer potential limits (see Fig. 2). In potential scans stopped at the upper potential limit complete stripping of the metal deposits was verified by scanning the electrode potential again after transfer of the stripped electrode to a cell containing the supporting electrolyte solution only.

In several cases the metal deposition process is less pronounced as, e.g., in the case of palladium deposition on pyrolytic graphite as shown in Fig. 3. With the same metal ion but a different substrate (glassy carbon activated electrochemically) a slightly different picture emerges (Fig. 4). With both substrate materials the actual deposition potential corresponds to the opd-modification.

Table 1 provides a list of the first deposition potentials encountered in a negative going potential scan as used during electrode modification. Because the deposition occurred almost independently of the substrate

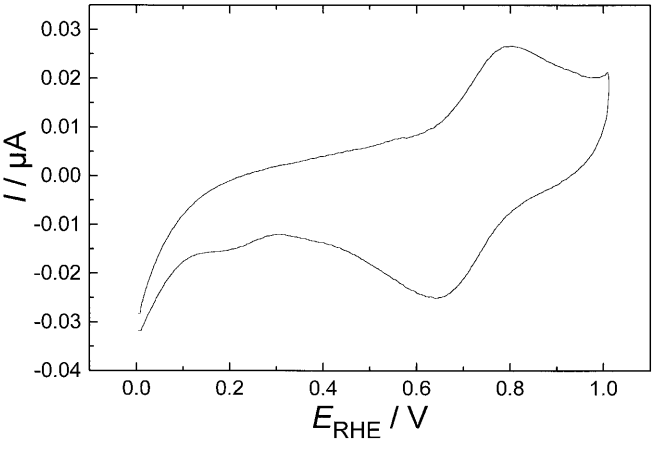

Fig. 1 Cyclic voltammogram of an electrode made of Elektrodengraphit EH, aqueous solution of 1 M $HClO_4$ + 1 mM $Pb(CH_3COO)_2$, $dE/dt = 5$ mV/s

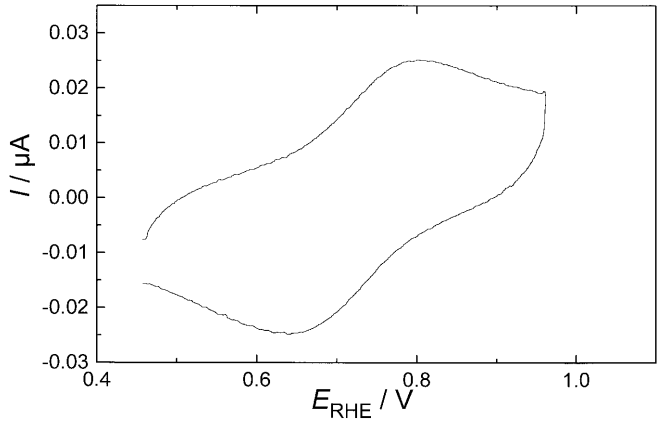

Fig. 2 Cyclic voltammogram of an electrode made of Elektrodengraphit EH, aqueous solution of 1 M $HClO_4$ + 1 mM $Pb(CH_3COO)_2$, $dE/dt = 5$ mV/s

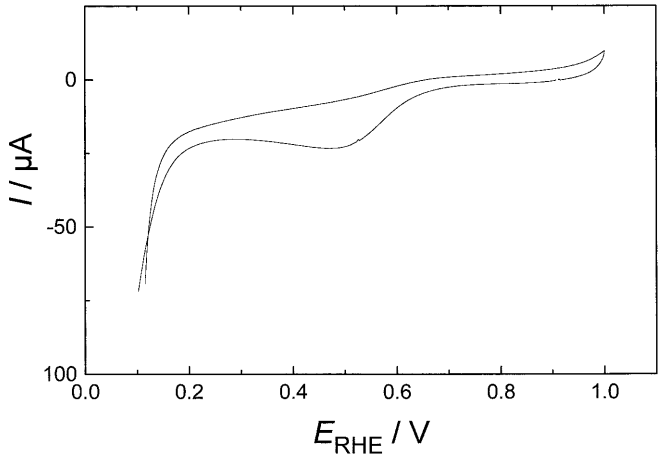

Fig. 3 Cyclic voltammogram of an electrode made of pyrolytic graphite, aqueous solution of 1 M $HClO_4$ + 1 mM $Pd(NO_3)_2$, $dE/dt = 5$ mV/s

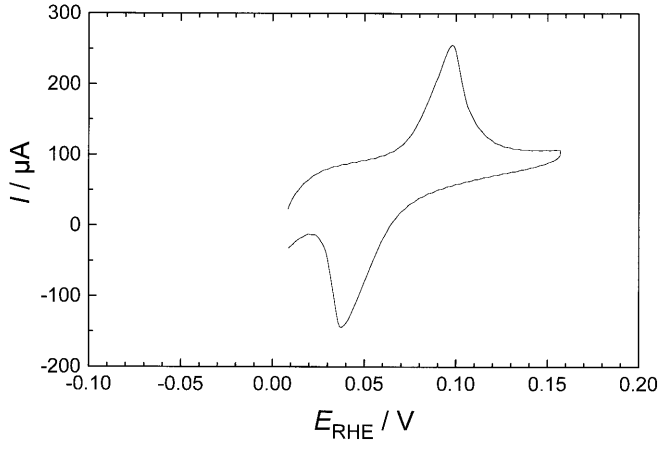

Fig. 4 Cyclic voltammogram of an electrode made of glassy carbon (activated electrochemically), aqueous solution of 1 M $HClO_4$ + 1 mM $Pd(NO_3)_2$, $dE/dt = 5$ mV/s

Table 1 Standard electrode potentials, Nernst potentials (based on the employed metal ion concentrations) and experimentally observed deposition electrode potentials of investigated metal ions

Metal	$E_{00,NHE}$ (V)	$E_{Nernst,NHE}$ (V)	$E_{depos.,RHE}$ (V)	Type of deposition
Ag^+	+0.799	+0.625	+0.58	opd
Bi^{3+}	+0.2	+0.141	+0.025	opd
Cd^{2+}	–0.403	–0.49	+0.16	upd
Co^{2+}	–0.28	–0.37	+0.15	upd
Cu^{2+}	+0.342	+0.25	+0.25	upd
Ni^{2+}	–0.257	–0.34	+0.50	upd
Pb^{2+}	–0.126	–0.21	–0.21	opd
Pd^{2+}	+0.951	+0.86	+0.037	opd
Pt^{2+}	+1.118	+1.03	+0.45	opd
Sn^{2+}	–0.137	–0.22	+0.55	upd
Tl^+	–0.336	–0.42	+0.57	upd
Zn^{2+}	–0.761	–0.85	+0.52	upd

material at the same potential for a given ion the list includes values obtained with all substrate materials. By comparison with the "Nernst potential" (standard potentials were taken from the literature [41]) calculated assuming the actual metal ion concentration in solution and an electrode of the same metal, the deposits are designed as being *opd* or *upd*. The repeatedly poorly developed CVs cause considerable uncertainty in determination of the deposition potentials (see e.g. Fig. 3). An attempt was made to calculate the charge consumed during metal deposition in order to determine the amount of metal being present on the substrate surface and subsequently to determine the degree of coverage q. Submonolayer coverages were found.

Their topography was investigated using scanning electron microscopy. The surface topography of an unmodified electrode surface as well as the nanoscopic dimensions of the metal deposit are evident in representative scanning electron micrographs as displayed in Fig. 5. In this system three-dimensional growth of the metal deposits occurred. The white spots observed with the electrochemically activated electrode indicate the presence of localized highly oxidized areas.

Impedance measurements were done with electrodes modified by metal deposits prepared without moving the electrode potential into the bulk deposition region. Impedance data for the $Fe^{(II)}/Fe^{(III)}$ redox couple at its rest potential E_0 were used to obtain charge transfer resistances R_{ct}. In a few cases E_0 was in a range where basically dissolution of the upd-layer may occur (i.e., positive to the upd-potential). A typical set of impedance data as obtained with an electrode of pyrolytic graphite is shown in Fig. 6. Respective data sets obtained with the other materials are displayed in Figs. 7, 8, 9, and 10.

Evaluation of the data was attempted by using a least squares fit procedure (see above) and a Randles-type equivalent circuit. Using a simple condenser-type element as a representation of the double layer capacitance resulted in rather unsatisfactory fits. Incorporating a constant phase element, CPE, with a capacitance and a factor n describing the deviation from the ideal

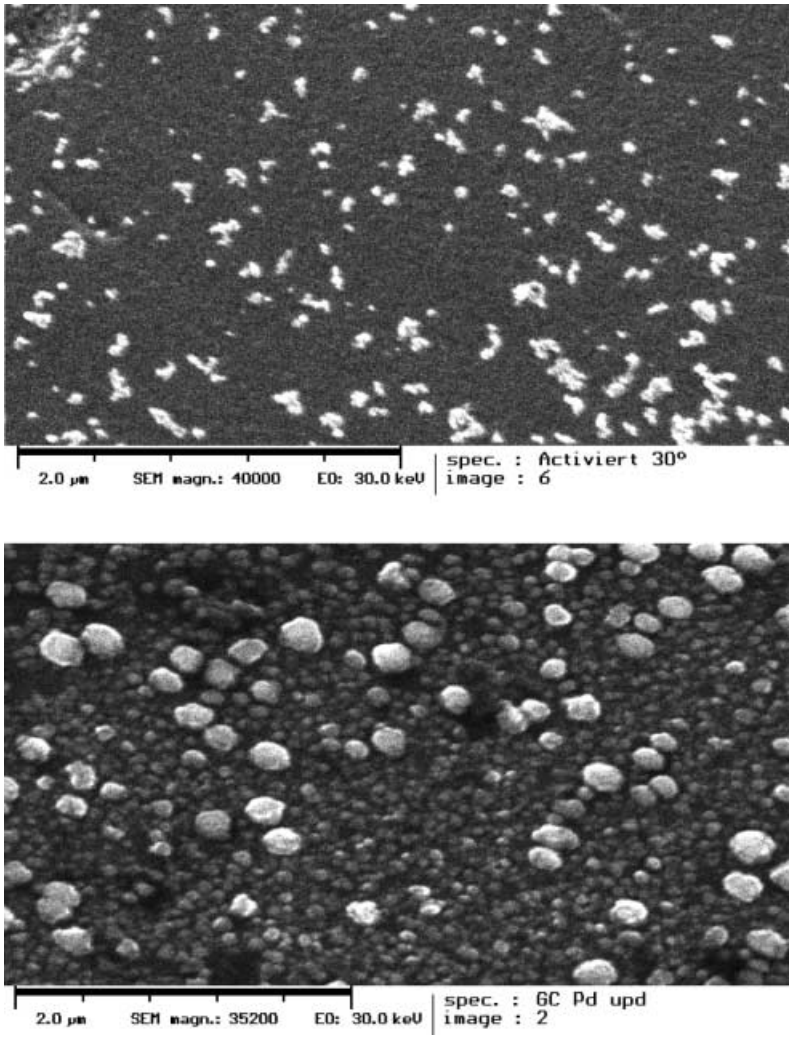

Fig. 5 Scanning electron microscope picture of a glassy carbon electrode after activation (*top*) and modified with palladium (*bottom*)

capacitive behaviour resulted in dramatic improvements. The concept of the CPE has been discussed elsewhere [42, 43, 44, 45, 46, 47, 48, 49, 50, 51, 52, 53, 54, 55, 56, 57]. Basically, this element takes into account surface inhomogeneities. These may be different surface properties, surface roughness, etc. Results of the fitting procedure are collected in Table 2; selected data and further kinetic results are collected for unmodified electrodes in Table 3. This table also contains kinetic data as derived from cyclic voltamograms, the data are in good agreement.

The electrolyte resistance was always included in the fitting procedure. The values are of no particular interest except for the fact that the values obtained with Ridurid were much larger as compared to the other materials because of the rather high percentage of electronically non-conducting phenolic resin in this material.

In order to compare the data obtained with different substrates a comparison of the double layer capacitance, which may be taken as a measure of the electrochemically active surface area [58], serves as a starting point.

Literature data on the specific double layer capacity as determined with a variety of electrochemical techniques including in a few cases additional information obtained with other surface analytical tools range from 3 $\mu F\ cm^{-2}$ for the basal plane of stress annealed pyrolytic graphite SAPG [59, 60] over 16 $\mu F\ cm^{-2}$ for the basal plane of polished ordinary pyrolytic graphite OPG [60], 25 $\mu F\ cm^{-2}$ for polished glassy carbon [61] up to 50 to 70 $\mu F\ cm^{-2}$ for edge-oriented, polished SAPG [60]. Some reported data are at slight variance. Bauer et al. [62] have reported a double layer capacitance of 12 $\mu F\ cm^{-2}$ for the freshly cleaved basal plane of OPG and a value of 60 $\mu F\ cm^{-2}$ for the same surface after polishing. In a fairly general investigation Gagnon [63] has observed a value of 10 $\mu F\ cm^{-2}$ for various carbons in an aqueous solution of KOH (31%). Soffer and Folman have calculated a value of 10 $\mu F\ cm^{-2}$ for activated carbon taking into account the BET surface as the true electrode surface [64]. The values of C_{DL} reported here (see Table 2) are well within this range.

In order to obtain at least an estimate of the degree of structural disorder of the investigated materials which may in turn be correlated with surface roughness, surface Raman spectra were evaluated [65]. Various literature reports were considered for comparison. Besides

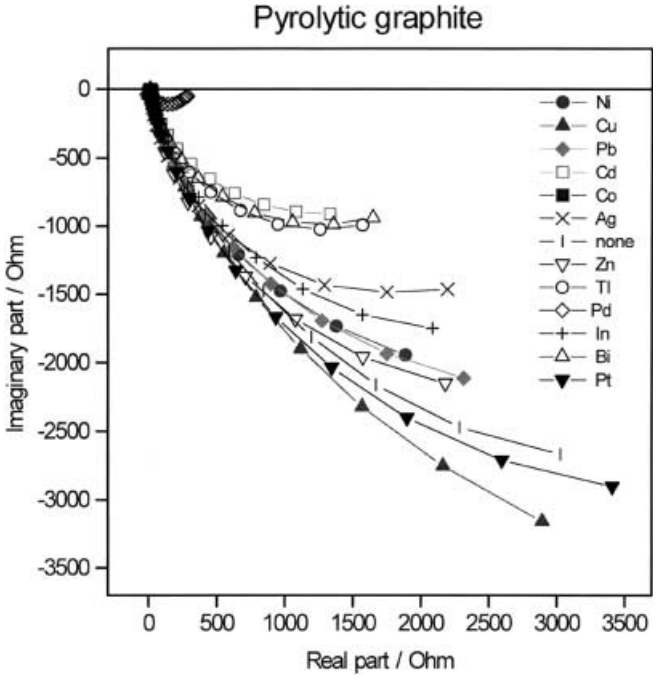

Fig. 6 Impedance data obtained with an electrode made of pyrolytic graphite, aqueous solution of 10^{-2} **M** $Fe(NH_4)_2(SO_4)_2$/ $Fe(NH_4)(SO_4)_2 + 1$ M $HClO_4$

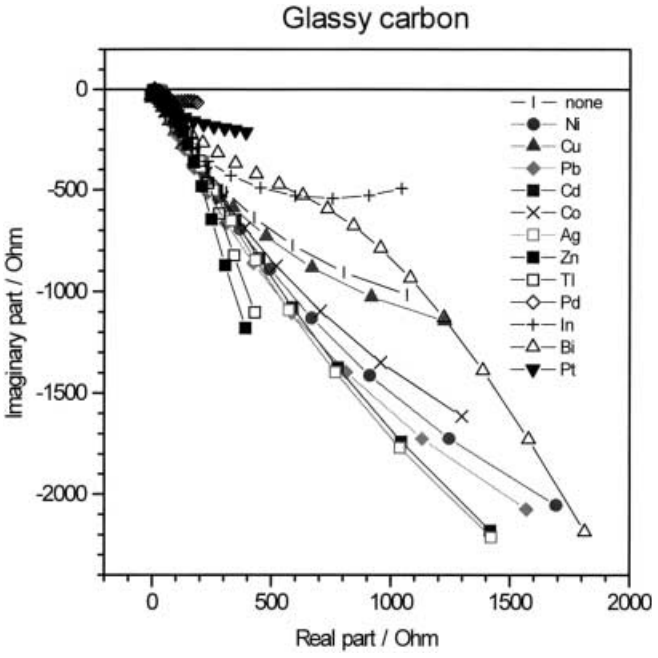

Fig. 8 Impedance data obtained with an electrode made of glassy carbon (electrochemically activated), aqueous solution of 10^{-2} M $Fe(NH_4)_2(SO_4)_2/Fe(NH_4)(SO_4)_2 + 1$ M $HClO_4$

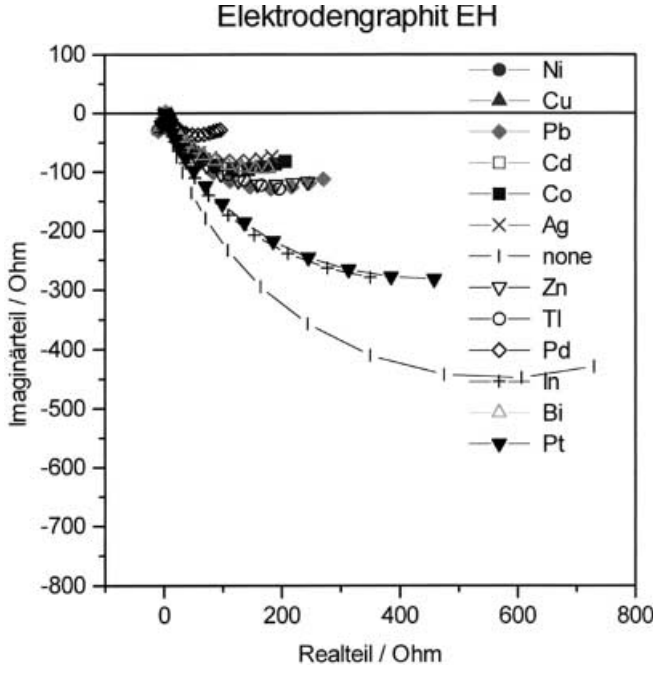

Fig. 7 Impedance data obtained with an electrode made of Elektrodengraphit EH, aqueous solution of 10^{-2} M $Fe(NH_4)_2(SO_4)_2/Fe(NH_4)(SO_4)_2 + 1$ M $HClO_4$

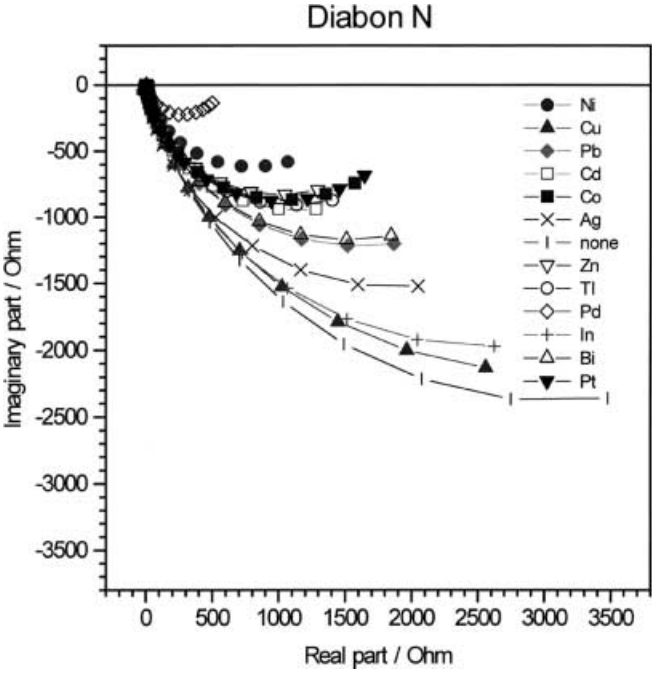

Fig. 9 Impedance data obtained with an electrode made of Diabon N, aqueous solution of 10^{-2} M $Fe(NH_4)_2(SO_4)_2/Fe(NH_4)(SO_4)_2 + 1$ M $HClO_4$

results implying predominantly an enhanced scattered intensity by means of, e.g., silver deposition [66, 67, 68, 69, 70], reports demonstrating the potential of Raman spectroscopy as a tool to detect lattice damage, etc., which in turn may affect the density of states at the surface involved in the electron transfer reaction, were evaluated [71, 72, 73, 74] The spectra reported within the present study are displayed in Figs. 11, 12, 13, 14, 15, and 16. Spectra of HOPG with the basal plane and the

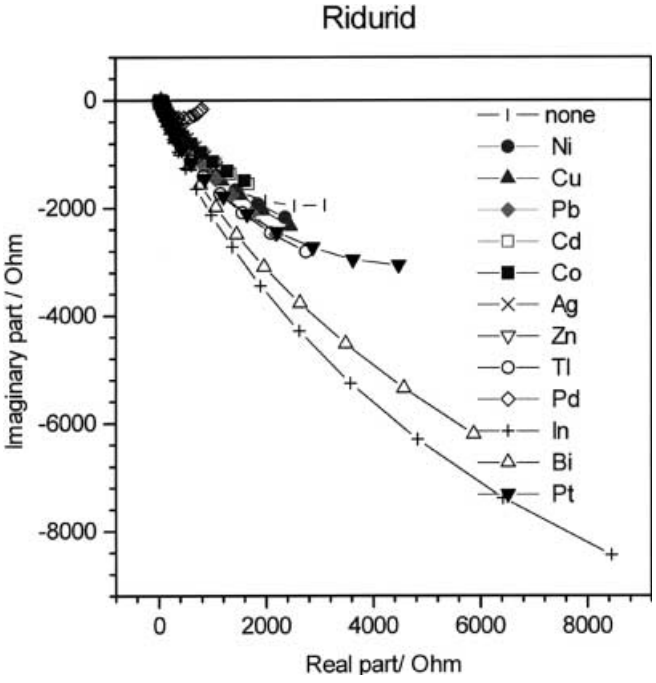

Fig. 10 Impedance data obtained with an electrode made of Ridurid, aqueous solution of 10^{-2} M $Fe(NH_4)_2(SO_4)_2/Fe(NH_4)(SO_4)_2 + 1$ M $HClO_4$

edge plane illuminated are shown for comparison in Figs. 17 and 18. The band at 1580 cm^{-1} in the spectrum of HOPG with the highly ordered basal plane illuminated has been assigned to the E_{2g} mode. A band around $\lambda = 1355$ cm^{-1}, attributed to the D or A_{1g} mode [72], is found in addition when the less well-ordered edge plane of HOPG is illuminated. By comparing spectra of the materials used in this work, some estimate of ordering should be possible. The spectrum of pyrolytic graphite (Fig. 11) resembles the spectrum of the edge plane of HOPG in a striking fashion. The value of the double layer capacitance displayed as the value of a CPE (for reasons of this assignment, see above) is very close to the value of polished OPG reported by Bauer et al. [62]. Unfortunately, no values are available for the double layer capacity of HOPG, consequently this number cannot be included in the comparison. The value of the CPE for PG nevertheless implies a fairly ordered structure and a smooth surface in agreement with the results of Raman spectroscopy.

With Elektrodengraphit EH only very weak spectra were obtained (Fig. 12). They show both bands but, because of the poor signal/noise ratio, any evaluation with respect to surface structure and roughness is not reasonable.

With glassy carbon even in its non-activated state the band around 1355 cm^{-1} indicating a disordered state is more intense than the band around 1600 cm^{-1} (Fig. 13). Assuming that such a disordering translates into a more irregular non-smooth surface, a large value of the CPE can be expected as a consequence; and this is indeed observed. Somewhat surprisingly, after the electro-

Table 2 Results of the fits of the impedance data

Metal	$R_{ct}(\Omega\ cm^{-2})$	CPE ($F\ cm^{-2}$)	n	F[a]
Pyrolytic graphite				
none	2974	5.96×10^{-5}	0.90	1
Ag	1601	6.64×10^{-5}	0.95	1.85
Bi	1111	8.80×10^{-5}	0.91	2.67
Cd	978	10.79×10^{-5}	0.91	3.04
Co	1514	12.08×10^{-5}	0.90	1.96
Cu	3434	5.85×10^{-5}	0.88	0.8
In	2041	9.14×10^{-5}	0.87	1.45
Ni	2114	9.06×10^{-5}	0.91	1.4
Pb	2243	7.22×10^{-5}	0.89	1.32
Pd	134	15.40×10^{-5}	0.92	22.19
Pt	3162	5.04×10^{-5}	0.88	0.94
Tl	1214	11.13×10^{-5}	0.90	2.45
Zn	2268	7.61×10^{-5}	0.93	1.31
Elektrodengraphit EH				
none	654	1.95×10^{-4}	0.82	1
Ag	58	11.91×10^{-4}	0.85	11.27
Bi	72	1.74×10^{-3}	0.78	9.08
Cd	75	12.51×10^{-4}	0.78	8.72
Co	75	1.19×10^{-3}	0.80	8.72
Cu	219	7.37×10^{-4}	0.80	2.98
In	194	1.00×10^{-3}	0.84	3.37
Ni	283	2.27×10^{-4}	0.80	2.31
Pb	104	10.68×10^{-4}	0.77	6.28
Pd	29	1.71×10^{-3}	0.8	22.18
Pt	207	7.28×10^{-4}	0.81	3.15
Tl	78	1.43×10^{-3}	0.8	8.38
Zn	87	0.99×10^{-3}	0.8	7.5
Glassy carbon (activated electrochemically)				
none	94	9.44×10^{-4}	0.77	1
Ag	57	9.51×10^{-4}	0.80	1.65
Bi	44	8.85×10^{-4}	0.81	2.13
Cd	266	1.12×10^{-4}	0.80	0.35
Co	71	1.29×10^{-3}	0.73	1.32
Cu	110	6.41×10^{-4}	0.82	0.85
In	313	5.05×10^{-4}	0.80	0.30
Ni	157	5.72×10^{-4}	0.82	0.59
Pb	83	1.69×10^{-3}	0.76	1.13
Pd	0.55	6.21×10^{-4}	0.84	170.90
Pt	81	10.40×10^{-4}	0.77	1.16
Tl	66	8.2×10^{-4}	0.79	1.42
Zn	36	2.11×10^{-3}	0.75	2.61
Diabon N				
none	1590	9.24×10^{-5}	0.87	1
Ag	968	1.45×10^{-4}	0.91	1.64
Bi	766	1.54×10^{-4}	0.89	2.07
Cd	594	2.27×10^{-4}	0.92	2.67
Co	548	1.42×10^{-4}	0.93	2.90
Cu	1341	1.23×10^{-4}	0.88	1.18
In	1257	1.16×10^{-4}	0.89	1.26
Ni	406	2.44×10^{-4}	0.89	3.91
Pb	802	1.55×10^{-4}	0.88	1.98
Pd	148	2.73×10^{-4}	0.92	10.74
Pt	552	1.23×10^{-4}	0.93	2.88
Tl	580	1.98×10^{-4}	0.92	2.74
Zn	530	2.16×10^{-4}	0.92	3.00
Ridurid				
none	1606	2.18×10^{-4}	0.80	1
Ag	2413	2.48×10^{-4}	0.72	0.66
Bi	76	3.38×10^{-3}	0.82	21.13
Cd	1903	1.25×10^{-4}	0.79	0.84
Co	1888	1.35×10^{-4}	0.78	0.85
Cu	2862	8.46×10^{-5}	0.79	0.56
In	9718	2.26×10^{-5}	0.84	0.16
Ni	2758	9.25×10^{-5}	0.80	0.58

Table 2 (Contd.)

Pyrolytic graphite				
Metal	R_{ct}(Ω cm^{-2})	CPE (F cm^{-2})	n	F[a]
Pb	3536	1.01×10^{-5}	0.77	0.45
Pd	393	8.66×10^{-5}	0.91	4.08
Pt	3425	3.67×10^{-5}	0.86	0.46
Tl	3355	7.11×10^{-5}	0.85	0.478
Zn	830	5.65×10^{-4}	0.80	1.93

[a]Catalytic enhancement factor relative to the unmodified electrode surface

chemical activation the ratio of the Raman bands is only slightly reduced (see Fig. 14) whereas a further increase of the CPE is registered.

The Raman spectrum of Diabon N differs considerably from those recorded with the other materials (Fig. 15). This is certainly caused in part by the resin used as binder and filler. In the displayed spectrum only the region discussed before with the other materials is considered, the band at lower wave numbers is higher indicating a highly disordered material. Because of the unknown fraction of the binder, which is electrically insulating and does not contribute to the establishment of the electrochemical double layer, the value of the CPE, which is very low, cannot be compared with values obtained for materials without filler.

The Raman spectrum of Ridurid (Fig. 16) is displayed for completeness only, the bands typical of carbon are barely visible.

With respect to the following discussion of conceivable relationships between structural, morphological or topographical features of the investigated carbons as evident from the Raman spectra and their electrocatalytic activity, PG is most likely the least active material, whereas of those samples yielding useful spectra, GC is less well ordered and most likely more active.

In previous reports of measurements with porous electrodes, the value of the double layer capacity was used as a measure of the amount of electrochemically active surface area within gas fed porous electrodes [58].

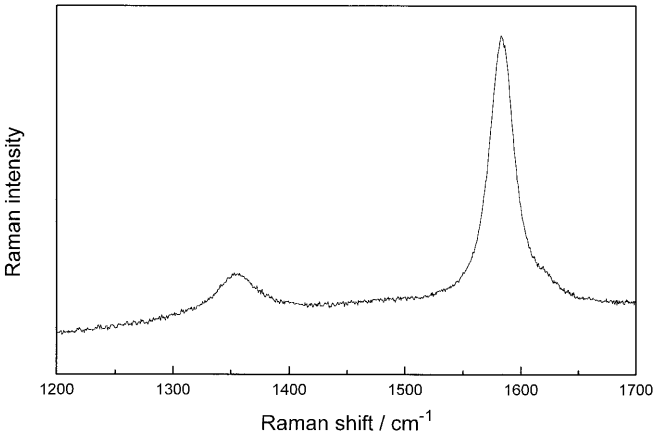

Fig. 11 Surface Raman spectrum of pyrolytic graphite, $\lambda_0 = 514.5$ nm, $p_{Laser} = 300$ mW

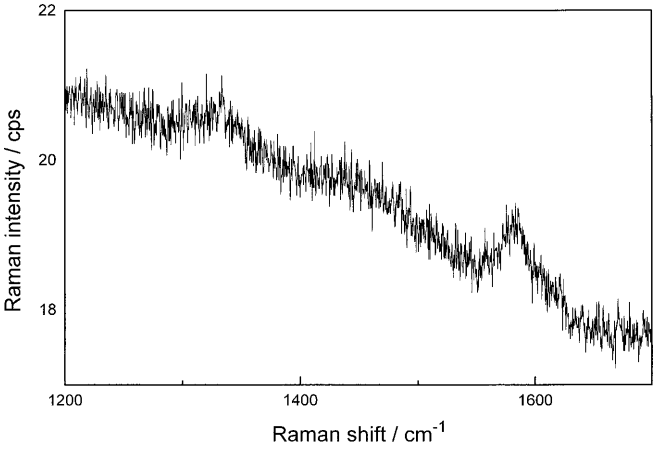

Fig. 12 Surface Raman spectrum of Elektrodengraphit EH, $\lambda_0 = 647$ nm, $p_{Laser} = 50$ mW

Table 3 Values of CPE, R_{ct}, j_0, j_{00}, and k_0 of investigated carbons without modification[a]

	CPE (μF cm^{-2})	R_{ct} (Ω cm^{-2})	j_0 (A cm^{-2})	j_{00} (A cm^{-2})	k^0 (cm s^{-1})	k^0 (cm s^{-1})[b]	k^0 (cm s^{-1})
Pyrolytic graphite	59	2974	8.5×10^{-6}	0.42	4.4×10^{-6}	5.9×10^{-6}	–
Elektroden-graphit EH	195	654	3.8×10^{-5}	1.9	2×10^{-5}	1.4×10^{-5}	–
Glassy carbon	–	–	–	–	–	–	1.02×10^{-3} [31]
Glassy carbon (activated electro-chemically)	944	94	2.7×10^{-4}	13.4	1.4×10^{-4}	1.1×10^{-4}	2.3×10^{-3} [30]
							8.6×10^{-2} [31]
Diabon N	92	1590	1.6×10^{-5}	0.8	8.2×10^{-6}	5.3×10^{-6}	–
Ridurid	218	1606	1.6×10^{-5}	0.8	8.1×10^{-6}	2.9×10^{-6}	–
HOPG (edge plane)	704	248	1.0×10^{-5}	0.5	5.3×10^{-6}	1×10^{-5}	–
HOPG (basal plane)	92*	–	–	–	–	1.5×10^{-5}	1.4×10^{-5} [30]

[a]Conversion relationships: $j_0 = (RT)/(nFR_{ct})$, $j_{00} = (j_0 c^*)/\left(c_{ox}^{\alpha}\, c_{red}^{1-\alpha}\right)$, $k^0 = j_{00}/(nFc^*)$ with: c^* as a standard concentration
[b]Data taken from cyclic voltammograms

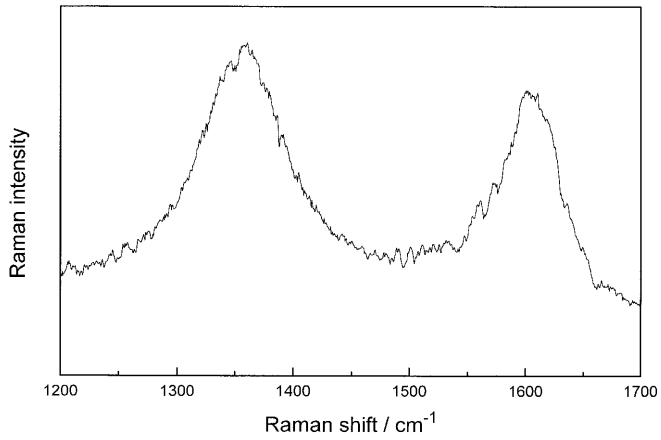

Fig. 13 Surface Raman spectrum of glassy carbon, $\lambda_0 = 647$ nm, $p_{\text{Laser}} = 200$ mW

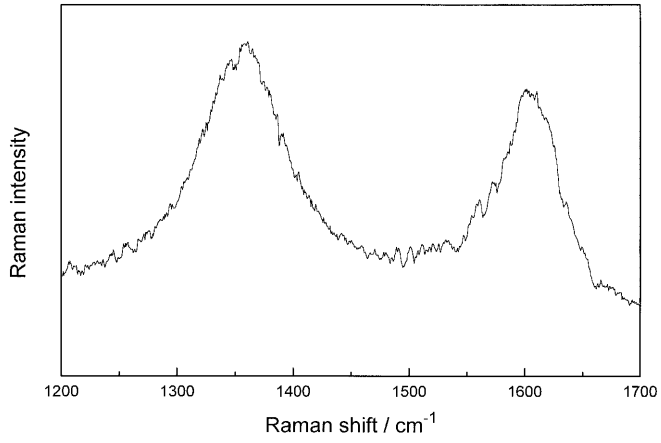

Fig. 14 Surface Raman spectrum of glassy carbon, activated, $\lambda_0 = 514.5$ nm, $p_{\text{Laser}} = 100$ mW

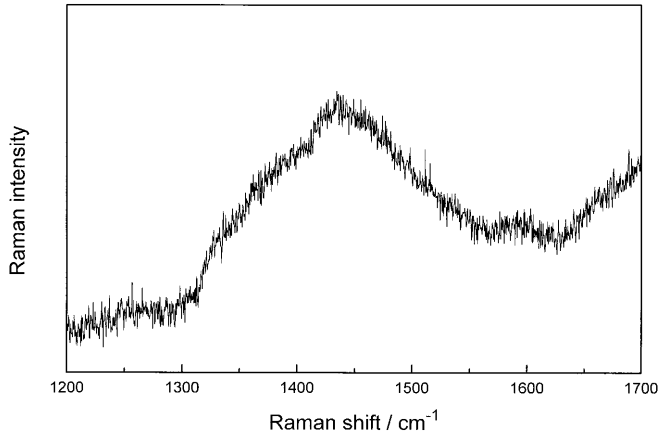

Fig. 15 Surface Raman spectrum of Diabon N, $\lambda_0 = 647$ nm, $p_{\text{Laser}} = 200$ mW

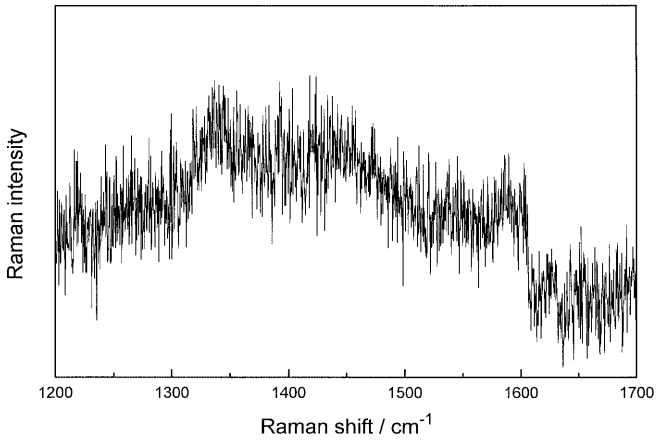

Fig. 16 Surface Raman spectrum of Ridurid, $\lambda_0 = 647$ nm, $p_{\text{Laser}} = 50$ mW

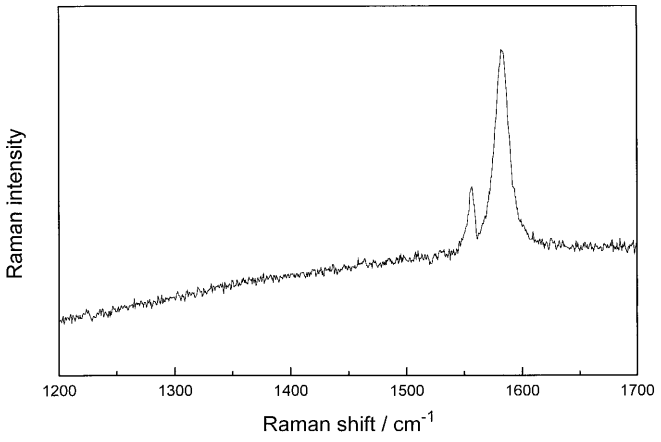

Fig. 17 Surface Raman spectrum of highly ordered pyrolytic graphite, basal plane, $\lambda_0 = 514.5$ nm, $p_{\text{Laser}} = 300$ mW

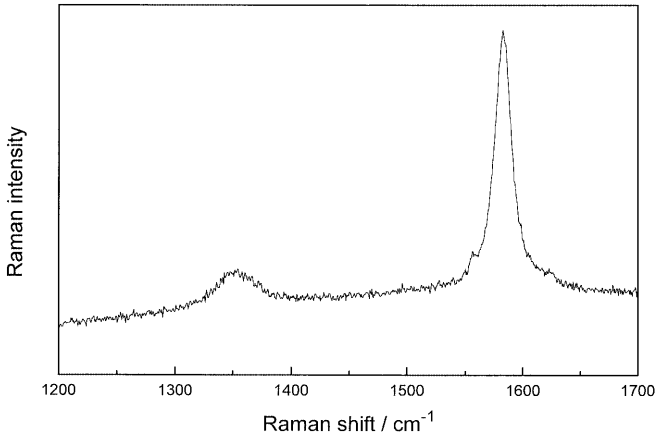

Fig. 18 Surface Raman spectrum of highly ordered pyrolytic graphite, edge plane, $\lambda_0 = 514.5$ nm, $p_{\text{Laser}} = 300$ mW

Comparing the typical micro- and mesoscopic dimensions of these porous electrodes and the dimensions of the surface roughness encountered here (tentatively excluding activated glassy carbon), the kinetic data obtained with the different materials with and without modification by metal deposits should be compared

based on the geometric surface area. An attempt to include the value of CPE by, e.g., normalizing the values of R_{ct} or j_0 with respect to the value of CPE would result in a highly speculative discussion. As listed in Table 3, the values of CPE and R_{ct} do not show a relationship suggesting such a correlation. This approach, i.e., the exclusion of CPE or the comparable value of the double layer capacity, has been found to be appropriate also with metal electrodes used in kinetic investigations with a turbulent pipe flow setup [75].

Comparing the values of R_{ct} and the derived values of j_0 and k^0 as listed in Table 3 shows glassy carbon after activation as the most active electrocatalyst. The value of k^0 is in acceptable agreement with results reported by McDermott et al. [30]. Despite the presence of presumably electrochemically inactive binding/filling material, the respective values of j_0 for Diabon N and Ridurid are not the lowest ones. Pyrolytic graphite turns out to show the lowest activity for the investigated redox reaction. The trend from lower values of j_0 for more ordered materials like, e.g., PG to higher values of j_0 with less ordered materials like, e.g., GC has been observed with a broad selection of redox systems by Cline et al. [76]. Bowling et al. have observed a correlation between the intensity of the A_{1g} mode of HOPG increased by, e.g., laser activation and the value of j_0 of various redox reactions [72, 77]. The A_{1g} was treated as an indicator of the density of defect states or edge plane states. Accordingly, an increase in the number of defects correlates with an enhanced rate of the electron transfer reaction. In turn, the low density of states and of charge carriers typical of the basal plane of HOPG corresponds to very low electron transfer rates [76]. The difference between the values of k^0 for the basal and the edge plane of HOPG as found with the redox system investigated here is at variance with literature data reported elsewhere (see, e.g., [77]), where considerably larger differences for other redox systems were found. Since the value of k^0 reported here for the $Fe^{(II)}/Fe^{(III)}$ redox couple for the basal plane of HOPG resembles closely the small value found by Bowling et al. [77] and other authors [74], this difference cannot be caused by surface defects of the used HOPG as suggested elsewhere [77]. Instead the low activity of the basal plane needs further investigation.

Kinetic data obtained with metal-modified electrodes indicate different metal-specific effects. With some metals a considerable decrease of R_{ct}, i.e. an increased activity is observed (e.g. ,Cd, Pd, depending on the type of carbon substrate used), with some metals no effect or even a decrease is found. The upd-layers show these effects even at electrode potentials positive to the upd-potentials; i.e., the layers are stable at these potentials. The increase of the electrochemically active surface area as probed by measuring the double layer capacitance is small, usually it is limited to a factor of 2 to 3. A constant phase element CPE with exponent n was used instead of a simple capacitor taking into account the three-dimensional shape of the electrochemical interface ($n = 1$ corresponds to a smooth surface). Consequently, true electrocatalytic effects can be identified. Catalytic enhancement factors F ($F = R_{ct,modif.}/R_{ct,unmodif.}$) relating R_{ct} with and without metal modification can be calculated. The actual values of F depend on the substrate, general tendencies are the same for all investigated substrates. A comparison of the reported results with previously published data pertaining to metal modified graphite/carbon electrodes, in particular those modified by upd-deposits, is almost impossible. As already indicated earlier by Kolb [78], most observations pertaining to metal deposits refer to the anodic stripping of metal deposits on graphitic substrates as employed for analytical purposes [79, 80, 81]. Nevertheless, details reported by Vassos and Mark [82] indicate at least the possibility of strong metal-graphite interaction as assumed as a prerequisite of upd-processes. Such an interaction, which in turn implies a two-dimensional deposit instead of the three-dimensional deposit as observed in some of the cases reported here, may not be controlling in the deposits formed within the work reported here at electrode potentials positive to the Nernst potential.

The particular activity of palladium-modified surfaces indicates a special role as already found in other electrocatalytic processes [83] without being understood completely so far. The catalytic effect is generally lower on composite materials containing inert binding materials. This may be in part caused by the fact that inert binding material cannot act as surface binding site for modifying metal deposits. With Ridurid in most cases an inhibiting influence of the metal deposit is found. Although the trend of the observed catalytic effects is basically the same for most of the investigated carbon materials, currently no explanation of the effect is available. A simple surface increase as a conceivable explanation can be ruled out based on the values of the double layer capacitance. Different electrosorption properties of the metals used for electrode modification are hardly a reasonable explanation, because the investigated electrode reaction is presumed to be an outer sphere reaction, consequently the metal should not show any significant influence at all. As the effects of the used metals are different depending on the electrode material, such an influence would be unlikely as a sole explanation in any case.

Acknowledgements Support of this work by the Deutsche Forschungsgemeinschaft, the Fonds der Chemischen Industrie and the Freistaat Sachsen is gratefully appreciated. Microscope pictures were acquired by S. Schulze.

References

1. Holze R, Fette U (1992) Dechema-Monographie, vol 125. VCH Verlagsgesellschaft, Weinheim, p 769
2. Holze R (1998) J Sol State Electrochem 2:73
3. Horozova E, Jordanova Z, Shterev G (1993) Electrochim Acta 38:1591
4. Takamura K, Sakamoto M (1980) J Electroanal Chem 113: 273

5. Cataldi TRI, Guerrieri A, Casella IG, Desimoni E (1995) Electroanalysis 7:305
6. Lain MJ, Pletcher D (1987) Electrochim Acta 32:109
7. Lain MJ, Pletcher D (1987) Electrochim Acta 32:99
8. Shibata M, Motoo M (1987) J Electroanal Chem 229:385
9. Motoo S, Watanabe M (1979) J Electrochem Soc 98:203
10. Furuya N, Motoo S (1976) J Electroanal Chem 72:165
11. Casella IG, Zambonin CG, Prete F (1999) J Chromatogr A 833:75
12. Cox JA, Dabek-Zlotorzynska E (1991) J Chromatogr 543:226
13. Dapperheld S (1988) Dechema-Monographie, vol 112. VCH Verlagsgesellschaft, Weinheim, p 317
14. Elshafei AA, Elmaksoud SAA, Fouda AS (1995) J Electroanal Chem 395:181
15. O'Connell PJ, O'Sullivan CK, Guilbault GG (1998) Anal Chim Acta 373:261
16. Castro-Luna AM, Iwasita T, Vielstich W (1985) J Electroanal Chem 196:301
17. Holze R, Castro-Luna A-M (1988) J Appl Electrochem 18:679
18. Yang CY (1982) J Appl Electrochem 12:425
19. Rodes A, Aldaz A, Garces P, Climent MA (1989) Bull Electrochem 5:129
20. Rüssel C, Krauß D, Ledjeff K (1986) Dechema-Monographie 102:139
21. Cnobloch H, Nischik H, Pantel K, Ledjeff K, Heinzel A, Reiner A (1988) Siemens Forsch Entwickl Ber 17:270
22. Cnobloch H, Nischik H, Pantel K, Ledjeff K, Heinzel A, Reiner A (1987) Dechema-Monographie 109:427
23. Cnobloch H, Nischik H, Pantel K, Ledjeff K, Heinzel A (19896) 4th Int Carbon Conf, Baden-Baden
24. Hruska LW, Savinell RF (1981) J Electrochem Soc 128:18
25. Johnson DA, Reid MA (1985) J Electrochem Soc 132:1058
26. Liu CC, Galasco RT, Savinell RF (1981) J Electrochem Soc 128:1755
27. Liu CC, Galasco RT, Savinell RF (1982) J Electrochem Soc 129:2502
28. Tsuda I, Kurokawa K, Nozaki K (1994) For a simulation of uses of redox batteries with photovoltaic systems. Sol Energ Mat Sol Cells 35:503
29. Kneten KR, McCreery RL (1993) J Electrochem Soc 140:2593
30. McDermott CA, Kneten KR, McCreery RL (1993) J Electrochem Soc 140:2593
31. Hollax E, Cheng DS (1985) Carbon 23:655
32. Kötz R, Barbero C, Schnyder B, Haas O (1993) Thin Solid Films 233:69
33. Otero L, Vettorazzi N, Barbero C, Miras MC, Silber JJ, Sereno L (1993) J Electroanal Chem 350:251
34. Barbero C, Kötz R (1993) J Electrochem Soc 140:1
35. Chen PH, McCreery RL (1996) Anal Chem 68:3958
36. Beilby AL, Sasaki TA, Stern HM (1995) Anal Chem 67:976
37. Holze R, Fischer G (1989) Dechema-Monographie 117:331
38. Holze R, Betowska-Brzezinska M (1985) Electrochim Acta 30:937
39. Nicholson RS (1965) Anal Chem 37:1351
40. Vidano RP, Fischbach DB (1981) Sol State Commun 39:341
41. D'Ans-Lax (1992) Taschenbuch für Chemiker und Physiker, Physikalisch-Chemische Daten, (Lechner MD, ed), Springer, Berlin 1992; p 474; CRC Handbook of Chemistry (Lide DR, ed), CRC Press, Boca Raton, 1997; Milazzo G, Caroli S (1978) Tables of standard electrode potentials, Wiley-Interscience, Chichester; The Encyclopedia of the Electrochemistry of the Elements (Bard AJ, ed), Marcel Dekker, New York, 1973
42. Okido M, Depo JK, Capuano GA (1993) J Electrochem Soc 140:127
43. Xue RJ, Huang H, Menetrier M, Chen LQ (1993) J Power Sources 44:431
44. Fawcett WR, Kovacova Z, Motheo AJ, Foss CA /1992) J Electroanal Chem 326:91
45. van Westing EPM, Ferrari GM, De Wit JHW (1994) Electrochim Acta 39:899
46. Bidoia ED, Bulhoes LOS, Rocha-Filho RC (1994) Electrochim Acta 39:763
47. MacDonald JR, Lehnen AP, Schoonman J (1982) J Electroanal Chem 131:77
48. Piela B, Wrona PK (1995) J Electroanal Chem 388:69
49. Bisquert J, Garcia-Belmonte G, Bueno P, Longo E, Bulhoes LOS (1998) J Electroanal Chem 452:229
50. Lang G, Heusler KE (1998) J Electroanal Chem 457:257
51. Lukacs Z (1999) J Electroanal Chem 464:68
52. Raistrick ID, Ho C, Huggins RA (1976) J Electrochem Soc 123:1469
53. Bottelbergs PH, Broers GHJ (1976) J Electroanal Chem 67:155
54. Wang YB, Yuan RK, Yuan H, Chen ZH (1993) Synth Met 55:1501
55. Goeminne G, Terryn H, Vereecken J (1995) Electrochim Acta 40:479
56. Wu XZ, Zhang WZ, Hou Y (1995) J Electroanal Chem 398:1
57. Sevastyanov AE, Stoinov Z (1992) Sov Electrochem (Engl Tr) 28:1117
58. Holze R, Vielstich W (1984) Electrochim Acta 29:607
59. Randin JP, Yeager E (1972) J Electroanal Chem 36:257
60. Randin JP, Yeager E (1971) J Electrochem Soc 118:711
61. Taylor RJ, Humffray AA (1973) J Electroanal Chem 42:342
62. Bauer HH, Spritzer MS, Elving PJ (1968) J Electroanal Chem 17:299
63. Gagnon EG (1975) J Electrochem Soc 122:521
64. Soffer A, Folman M (1972) J Electroanal Chem 38:25
65. For overviews, see: Nikiel L, Jagodzinski PW (1993) Carbon 31:1313; Fitzer E, Rozploch F (1988) High Temp-High Press 20:449 (1988); Nemanich RJ, Solin SA (1979) Phys Rev B 20:392; Tuinstra F, Koenig JL (1970) J Chem Phys 53:1126; Tuinstra F, Koenig JL (1970) J Composite Materials 4:492
66. Alsmeyer YW, McCreery RL (1991) Langmuir 7:2370
67. Alsmeyer YW, McCreery RL (1991) Anal Chem 63:1289
68. Zoval JV, Biernacki PR, Penner RM (1996) Anal Chem 68:1585
69. Zoval JV, Stiger RM, Biernacki PR, Penner RM (1006) J Phys Chem 100:837
70. See also: Rubim JC, Kannen G, Schumacher D, Dünnwald J, Otto A (1989) Appl Surf Sci 37:233
71. Alsmeyer DC, McCreery RL (1992) Anal Chem 64:1528
72. Bowling R, Packard R, McCreery RL (1988) J Electrochem Soc 135:1605
73. Rice RJ, McCreery RL (1989) Anal Chem 61:1637
74. Robinson RS, Sternitzke K, McDermott MT, McCreery RL (1991) J Electrochem Soc 138:2412
75. Iwasita T, Schmickler W, Herrmann J, Vogel U (1983) J Electrochem Soc 130:2026
76. Cline KK, McDermott MT, McCreery RL (1994) J Phys Chem 98:5314
77. Bowling RJ, Packard RT, McCreery RL (1989) J Am Chem Soc 111:1217
78. Kolb DM (1978) In: Advances in electrochemistry and electrochemical engineering, vol 11. (Gerischer H, Tobias CW, eds) Wiley, New York, p 125
79. Perone SP (18963) Anal Chem 35:2091
80. Brainina Z, Zakharchuk F, Synkova DP, Yudelevich IG (1972) J Electroanal Chem 35:165
81. Morcos I (1975) J Electroanal Chem 66:250
82. Vassos BH, Mark HB (1967) J Electroanal Chem 13:1
83. Burke LD, Casey JK (1993) J Electrochem Soc 140:1284